AIP | Review of Scientific Instruments

# Efficient spin resolved spectroscopy observation machine at Hiroshima Synchrotron Radiation Center

Taichi Okuda, Koji Miyamaoto, Hirokazu Miyahara, Kenta Kuroda, Akio Kimura et al.

Citation: Rev. Sci. Instrum. **82**, 103302 (2011); doi: 10.1063/1.3648102
View online: http://dx.doi.org/10.1063/1.3648102
View Table of Contents: http://rsi.aip.org/resource/1/RSINAK/v82/i10
Published by the American Institute of Physics.

# Efficient spin resolved spectroscopy observation machine at Hiroshima Synchrotron Radiation Center

Taichi Okuda,[1,a)] Koji Miyamaoto,[1] Hirokazu Miyahara,[2] Kenta Kuroda,[2] Akio Kimura,[2] Hirofumi Namatame,[1] and Masaki Taniguchi[1,2]
[1]*Hiroshima Synchrotron Radiation Center (HSRC), Hiroshima University, 2-313 Kagamiyama, Higashi-Hiroshima 739-0046, Japan*
[2]*Graduate School of Science, Hiroshima University, 1-3-1 Kagamiyama, Higashi-Hiroshima 739-8526, Japan*

(Received 31 July 2011; accepted 15 September 2011; published online 21 October 2011)

Highly efficient spin- and angle-resolved photoelectron spectrometer named ESPRESSO (Efficient SPin REsolved SpectroScopy Observation) machine has been developed at the beamline BL-9B in Hiroshima Synchrotron Radiation Center. Combination of high-resolution hemispherical electron analyzer and the high-efficient spin detector based on very low energy electron diffraction by the ferromagnetic target makes the high-energy resolution and angular resolution compatible with spin- and angle-resolved photoemission (SARPES) measurement. 7.5 meV in energy and $\pm 0.18^{\circ}$ in angular resolution have been achieved with spin resolution. The ESPRESSO machine, combination of quick energy-band dispersion measurement and Fermi surface mapping by two-dimensional electron detector for the spin integrated ARPES and the high-efficient spin analysis by the efficient spin detector realizes the comprehensive investigation of spin electronic structure of materials.  [doi:10.1063/1.3648102]

## I. INTRODUCTION

Electronics using the spin degree of freedom of electron, spintronics, has attracted much attention as the next generation electronics which can overcome the limitation of the existing charge utilizing devices. Spin- and angle-resolved photoelectron spectroscopy (SARPES) which can directly observe the spin-resolved band dispersions, is one of the most suitable and powerful experimental techniques to investigate the spin-related materials for the spintronic devices. As the discovery of the high-Tc superconductors promoted the development of high-resolution angular resolved photoelectron spectroscopy (ARPES), recent discovery of peculiar spin-texture of surface states by the spin-orbit interaction, such as surface Rashba spin splitting state or helical spin state of topological insulators stimulates to develop high-performance SARPES.

In this context, various kinds of new SAPRES apparatuses as well as conventional SARPES apparatuses which combine the electron analyzer with Mott type spin polarimeter[1] have been developed recently. For example, one of the outstanding SARPES systems named COPHEE (COmplete PHotoEmission Experiment) machine has been developed in Swiss Light Source (SLS) by the group of University of Zürich.[2] The COPHEE machine is equipped with two Mott detectors which are orthogonally placed to each other. Since each Mott detector can measure the spin with two quantization axes (x and z, and y and z) one can obtain the full 3D spin orientation by the machine. With the 3D spin detector and the motor-driven five axes goniometer one can measure band dispersion or Fermi surface of materials with the resolution of 3D spin orientation. Although the efficiency of Mott detector is usually very low, high brilliance of the photon beam from the undulator beamline of third generation synchrotron radiation (SR) light source at SLS makes the relatively high energy and angular resolution ($\Delta E \sim 70$ meV, and $\Delta\theta \sim \pm 0.5^{\circ}$) compatible with the 3D spin analysis.[3]

Without the high brilliance light from SR light source, brilliant laboratory sources using rare-gas plasma are now commercially available. By utilizing the large hemispherical analyzer with the compact Mott detector, the very high-energy resolution of about 8 meV with spin resolution has been reported by the help of brilliant Xe plasma lamp although the angular resolution is relatively poor ($\pm 1.5^{\circ}$).[4]

Utilizing these new apparatuses some observations of topological insulators with spin resolution have been reported already.[5,6] The limited angular and/or energy resolution of these apparatuses by the low efficiency of the Mott detector, however, hampers the discrimination of the tangled electronic structures such as proximal two spin states of $Bi_{1-x}Sb_x$ (Ref. 5) or faint spin modification of $TlBiSe_2$ by the Fermi surface warping effect[6] in which $\sim 0.05$ Å$^{-1}$ or better momentum resolution is required.

In order to overcome the disadvantage of the Mott detector and improve the efficiency of the SARPES measurement, some groups[7,8] employ time-of-flight (TOF) electron analyzer for the SARPES measurement, which one can measure electrons with wide range of kinetic energy at once and can reduce the acquisition time in principle. However, the necessity to use the pulse exciting light for the TOF measurement prevents one from utilizing the advantage of the high efficiency of the TOF measurement sufficiently.

The other approach to improve the efficiency of the SARPES measurement is to develop a spin detector which has higher efficiency than the Mott detector. The very low energy electron diffraction (VLEED) spin detector is one of such a high-efficient spin detectors which has been developed in 1989 for the first time[9] and successfully used for the

a)Electronic mail: okudat@hiroshima-u.ac.jp.

 

investigation of magnetic materials in the early days of development.[10] The problem of the quick degradation of the ferromagnet target for the VLEED detector has been overcome by utilizing the preoxidized Fe(001)-p(1×1)-O target[11] and put into practical use recently.[12–15] Because of the higher scattering probability of the low energy electrons ($E_k \sim$ 6–10 eV) compared with the high energy electrons ($E_k \sim$ 20–100 keV) for the Mott scattering and the relatively higher spin-resolving power of the method, almost two orders of higher efficiency than the conventional Mott detector has been reported so far[13,16] and applied to ravel the complex spin structure of $Bi_{1-x}Sb_x$.[17] Very recently, a novel SARPES machine combined both the VLEED detector and the TOF analyzer has also been reported.[8]

Even though the efficiency of the spin detection has been improved by using the VLEED spin detector, it is still quite lower than that of the spin-integrated ARPES measurement using 2D electron detector. Thus, it is very useful to grab quickly the spin-integrated electronic structure by efficient ARPES measurement using 2D detector and observe the spin structure at the specific position of **k**-space. This kind of approach has been done by using conventional Mott detector combined with hemispherical electron analyzer with 2D detector, recently.[4,18]

In this paper, we report our newly developed high-efficient SARPES apparatus named ESPRESSO (Efficient SPin REsolved SpectroScopy Observation) machine at the beamline BL-9B of Hiroshima Synchrotron Radiation Center (HSRC) in which the advantage of the high efficiency of the VLEED spin detector and the two-dimensional electron detection for the spin-integrated ARPES measurement has been combined for the first time. We have achieved SARPES measurement with very high energy- and angular-resolution ($\Delta E = 7.5$ meV and $\Delta\theta = \pm 0.18^\circ$) by the combination of state-of-the-art high-resolution hemispherical electron analyzer with the efficient spin detector based on the VLEED spin polarimeter. The quick band observation by the 2D detector of ARPES system and the rapid and precise spin structure observation realized by the high spin resolving power of VLEED will help the comprehensive understanding of electronic structures of spin-related materials.

## II. DESIGN OF THE ESPRESSO MACHINE

Schematic design of the ESPRESSO machine is shown in Fig. 1. As in the figure, the spin detector is connected via 90° electron deflector ($D_{EF}$) to the high-resolution hemispherical electron analyzer with a 200 mm mean radius (VG-Scienta R4000) which is modified for the ESPRESSO machine. Center part of photoelectrons which are energy analyzed by the hemispherical analyzer are detected with the two-dimensional detector (multi-channel plate: MCP (M)) and observed by a CCD camera via phosphor screen (P) for the spin-integrated ARPES measurement. Although the size of the MCP is 25 mm in diameter and smaller than the original one for normal VG-Scienta R4000 analyzer in which the diameter of the MCP is 40 mm, one can obtain ARPES band dispersion image with ±15° at once by the wide acceptance angle lens of the modified analyzer. The acceptance angle can be changed by

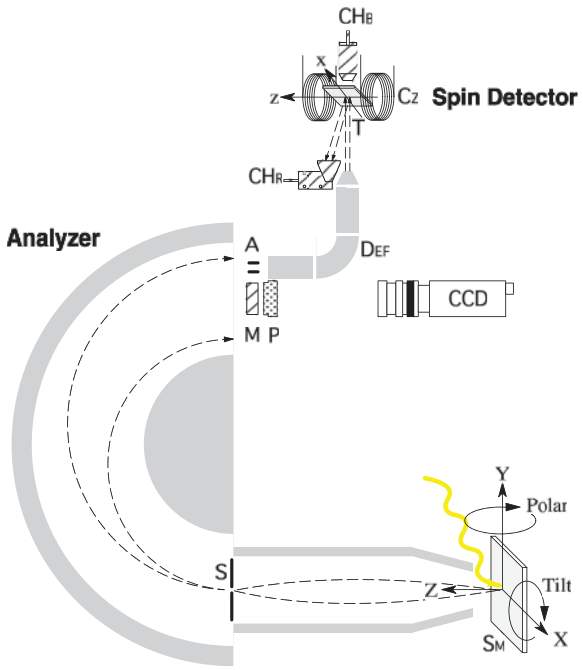


FIG. 1. (Color online) Schematic diagram of ESPRESSO machine. The highly efficient VLEED spin detector is connected to high-energy resolution hemispherical analyzer (VG-SCIENTA R4000) via 90° electron deflector ($D_{EF}$). The ferromagnetic target (T) can be magnetized by electric coils along z ($C_z$) and x ($C_x$; not shown in the figure) directions. The reflected electrons by the target are detected by the channeltron ($CH_R$) beside the exit of the deflector. By using the electron deflector both in-plane (x direction) and out-of-plane (z direction) spin components can be observed. Spin-integrated ARPES measurement is also available by observing the portion of photoelectron with the two-dimensional electron detector, multi-channel plate (MCP: (M)), and phosphor screen (P), through a CCD camera. Since the size of the aperture (A) for the spin-resolved measurement channel and the entrance slit (S) is variable, one can select the optimum energy resolution and angular resolution for the SARPES measurement.

using different lens modes to ±7.0° and ±3.5° for the high-angular resolution measurement. After the electrostatic lens the size variable entrance slit (S) is located as in the figure.

A part of electrons are further transferred to the spin detector via 90° deflector ($D_{EF}$) through small aperture (A) in which one can choose the optimum aperture size from some sets of apertures without breaking ultra-high vacuum (UHV). As in Table I, the angular resolution for the spin detection is in proportion to the transverse size of apertures. At the same time the energy resolution for the spin detection is dependent on the longitudinal aperture size and the entrance slit size. Expected energy resolution convoluting the resolution determined by the sizes of entrance slit and the aperture as well as some experimentally estimated ones are listed in Table II. Since the energy resolution is almost proportional to the analyzer pass energy ($E_p$), only the values for the $E_p = 2$ eV are listed.

The spin detector utilized here is the VLEED detector[9,16] in which Fe(001)-p(1×1)-O film fabricated on MgO(001) substrate is used as a target.[12–14] Low energy electrons whose energy is regulated to $E_k \sim 6$ eV are reflected by the magnetized target (T) and counted by the channeltron ($CH_R$) just beside the electron lens exit. The angle and position of the target can be adjusted by two sets of swivels and x-y stages

TABLE I. Angular resolution of SARPES measurement as the function of electron acceptance angle in different analyzer lens mode with different aperture size for spin detection channel. One can select optimum acceptance angle for spin-integrated ARPES and aperture size for SARPES according to the experimental requirement.

| | Aperture | | | |
|---|---|---|---|---|
| Lens acceptance | $\phi$ 4 | 2 ×3 | 1 ×2 | 0.5 ×1 |
| ±15° (Angular30) | ±3 | ±1.5 | ±0.75 | ±0.38 |
| ±7.5° (Angular14) | ±1.4 | ±0.70 | ±0.35 | ±0.18 |
| ±3.8° (Angular7) | ±0.70 | ±0.35 | ±0.18 | ±0.09 |

(Kohzu Precision Co. Ltd.) and one can easily find the best condition for getting the highest intensity of reflected electrons. The magnetization of the target along x and z directions in the figure can be done with electric coils (Cx and Cz, Cx is not drawn for the simplicity in the figure) which are orthogonally placed besides the target. The magnetization directions of the target correspond to the quantization axes of x and z directions of sample ($S_M$) coordination. Thus, we can measure both in-plane and out-of-plane spin components of observing sample. We have also the other channeltron ($CH_B$) under the target and can measure the intensity of incoming electrons into target position when we remove the target from the receptor.

The Fe(001)-p(1×1)-O film is fabricated in the target preparation chamber which is connected to the VLEED spin detector chamber and can be transferred into the spin detector without breaking UHV. In the target preparation chamber, Fe evaporator, oxygen doser, and target heating stage with target bank are equipped. Thus, one can prepare or refresh the target quickly. The detailed procedure of the target preparation has been reported in Ref. 13.

The SARPES machine is installed to the UHV chamber which is equipped with five axes (x, y, z, polar, and tilt angles) goniometer with cryostat (i-GONIO, AVC Co. Ltd.) which can cool the sample down to less than 10 K. Samples can be transferred from the UHV compatible preparation chamber which is equipped with surface preparation apparatuses such as low energy electron diffraction (LEED), reflected high-energy electron diffraction (RHEED), cylindrical mirror analyzer for Auger electron spectroscopy, ion-sputter-gun, metal evaporators, gas dosers, and sample manipulator with sample cooling (~80 K) and heating (~1600 K).

TABLE II. The calculated energy resolution of SARPES measurement as the function of the aperture and the entrance slit sizes at the analyzer pass energy of $E_p = 2$ eV. Note that the expected energy resolution is proportional to the analyzer pass energy and those for the different pass energies are not indicated. The experimentally determined energy resolution of some setups is also indicated in the parentheses. The energy resolution is governed by the entrance slit in case of the larger aperture size and vice versa.

| | Aperture | | | |
|---|---|---|---|---|
| Slit (mm) | $\phi$ 4 | 2 ×3 | 1 ×2 | 0.5 ×1 |
| 0.2 | 18.4 meV (11.4 ± 1.1) | 14.0 | 9.3 (7.4 ±0.6) | 4.9 |
| 0.5 | 18.6 (11.5 ± 2.3) | 14.2 | 9.5 (8.3 ±1.5) | 5.4 |
| 1.5 | 19.9 (21.2 ± 1.8) | 15.9 | 11.9 (10.3 ±1.2) | 8.9 |
| 4 | 27.2 (32 ± 2) | 24.4 | 22.0 (20 ±1.8) | 20.6 |

Whole ESPRSSO machine is installed at the multi-mode undulator beamline BL-9B of Hiroshima Synchrotron Radiation Center (HSRC). At the beamline, one can use SR light with linear or circular polarization monochromated by the dragon type grazing incidence monochromator in the energy range from 16 to 300 eV.[19] Laboratory light sources, He ($h\nu$ = 21.22 eV) and Xe discharge lamps ($h\nu$ = 8.437 eV), are also available for the offline measurement.

## III. PERFORMANCE OF THE ESPRESSO MACHINE

In order to estimate the performance of the ESPRESSO machine, we have measured Bi(111) single crystal thin film grown on Si(111) surface[20] as the test sample. Figure 2(a) shows the result of the Fermi surface mapping of the Bi(111) taken with the two-dimensional detector of ESPRESSO machine for the spin-integrated ARPES measurement with He discharge lamp ($h\nu$ = 21.22 eV). The typical Fermi surface structure of Bi(111), the electron pocket with hexagonal shape and petal-like six-fold hole pockets, is observed as reported in the previous study.[21] The band dispersions of the electron and hole pockets which are spin-polarized by the Rashba effect[21] are clearly seen in $E - k_{//}$ map along $\bar{\Gamma}$–$\bar{M}$ direction as in Fig. 2(b).

Spin-structure of any binding energy at any position in $k_x$-$k_y$ plane can be measured by tuning the energy of electron analyzer, and polar and tilt angles of goniometer. Figure 3 is one of the examples of such a SARPES data taken at the $k$ position marked by dotted circle in Fig. 2(a) which corresponds to the area between vertical dotted lines at about −0.1 $Å^{-1}$ in Fig. 2(b). In Fig. 3, upper panel shows the raw spectra taken with the target magnetization of plus ($I^+$: (red) solid line) and minus ($I^-$: (blue) dashed line). The spin up ($I^\uparrow$: (red) solid line) and spin down ($I^\downarrow$: (blue) dashed line) spectra in the middle panel are obtained by the usual procedure, $I^{\uparrow,\downarrow} = (1 \pm P)(I^+ + I^-)/2$ using the spin polarization $P$ (lower panel) determined as $P = \frac{1}{S_{eff}} A$. Here, $A$ is observed asymmetry between $I^+$ and $I^-$ spectra which is determined as $A = (I^+ - I^-)/(I^+ + I^-)$ and $S_{eff}$ is the effective Sherman function.

By comparing the observed asymmetry, $A$, by the ESPRESSO machine with the polarization, $P$, obtained by our old SARPES system[22] with the self-calibrated Mott detector, we can estimate the effective Sherman function ($S_{eff}$) of ESPRESSO machine as about 0.21 in this measurement. Although the $S_{eff}$ can change with different Fe(001)-p(1×1)-O target from time to time, one can calibrate the $S_{eff}$ by measuring the Bi(111) as the standard sample and we have found that the variation of the $S_{eff}$ of our targets is typically in between 0.2 and 0.4.

Although the Fe(001)-p(1×1)-O target is quite stable and one can use the same target more than several months, since the performance of the VLEED spin detector is sensitive to the target condition (surface cleanliness, roughness, and so on) and electron kinetic energy dependent, one should check

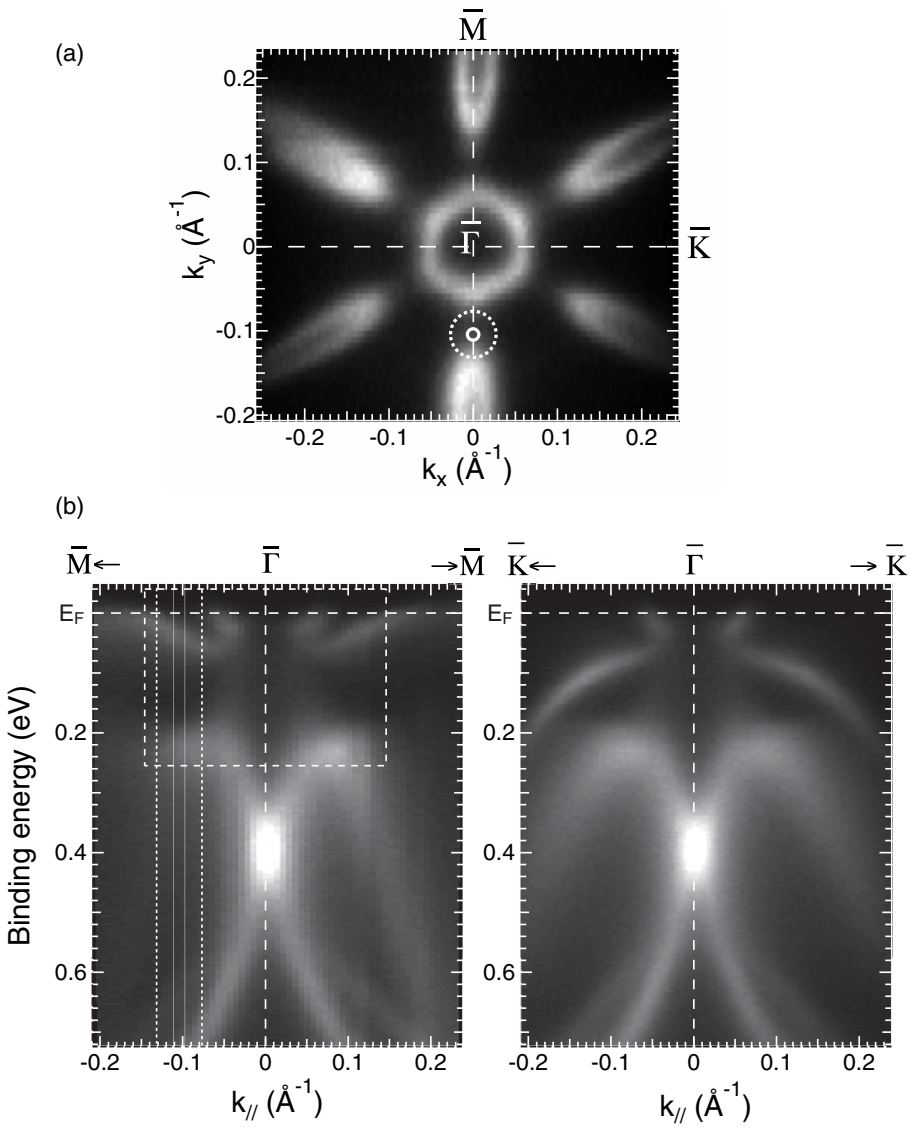


FIG. 2. (a) Fermi surface mapping of the Bi(111) film obtained by the two-dimensional detector of spin-integrated ARPES mode with the He discharge lamp ($h\nu = 21.22$ eV). (b) Electron band dispersions of Bi(111) film along $\bar{\Gamma}$–$\bar{M}$ (left) and $\bar{\Gamma}$–$\bar{K}$ (right) directions which correspond to the vertical and horizontal dashed lines in (a).

the best measurement condition, i.e., the best electron kinetic energy to operate, after the preparation of the new target. Figure 4 is one of the results of such an performance test for the target. For the test, we used the spin-polarized photoelectrons emitted from the strongest peak ($E_B = 2.43$ eV) of Bi film at ($k_x$, $k_y$)= (0, 0.236Å$^{-1}$). Note that the peak has similar electronic state to the strongest peak in Fig. 3 at $E_B = 2.60$ eV but the polarization is negative because of the Rashba effect in which the spin polarization is reversed against $\bar{\Gamma}$ point. As in the upper panel of Fig. 4, first we measure the intensity of reflected electrons by positively ($I^+$) and negatively ($I^-$) magnetized target as a function of electron kinetic energy at the target. To know the reflectivity of the electrons by the target the intensity of incoming electron ($I_0$) at the target position is measured by back channeltron ($CH_B$) in advance. Thus, one can estimate the reflectivity by the target $I/I_0 = (\frac{I^+ + I^-}{2})/I_0$ as in the second panel of Fig. 4. As mentioned already, from the $I^+$ and $I^-$ the asymmetry, $A$, of the reflected electrons between positively and negatively magnetized target can be obtained as $A = (I^+ - I^-)/(I^+ + I^-)$. Since the observed asymmetry $A$ is proportional to the effective Sherman function, $S_{eff}$, we can obtain the energy dependence of the $S_{eff}$ as in the third panel by the aforementioned calibration comparing the observed asymmetry data with that obtained by our Mott detector. With these $S_{eff}$ and $I/I_0$ we can estimate the total performance, the figure of merit which is defined as $I/I_0(S_{eff})^2$ as in the lowest panel, and the best FOM is estimated as $1.13 \times 10^{-2}$ at the kinetic energy of about 5.8 eV for this target. The value is about 100 times higher than typical Mott detectors and comparable to the previously reported VLEED detectors.[13,14,16]

This high efficiency of the spin detector combining with the state of the art hemispherical analyzer allows us to do high energy- and angular-resolution SARPES measurement. As an example, in Fig. 5 we show the high-resolution SARPES observation of the surface states of Bi(111) film.

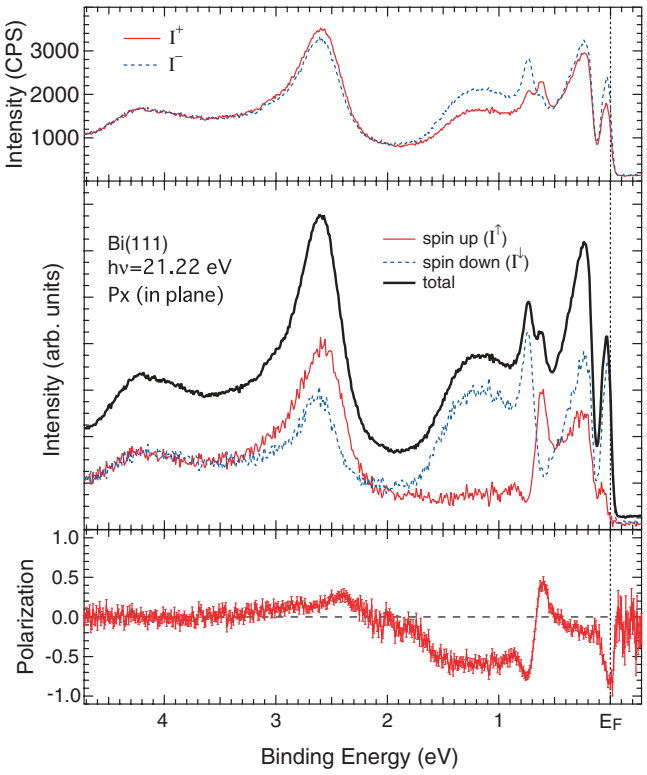


FIG. 3. (Color online) (Upper panel) Row SARPES spectra of Bi(111) film taken with plus ($I^+$: (red) solid line) and minus ($I^-$: (blue) dashed line) magnetized target at the specific $k$ point that is indicated by dotted circle in Fig. 2(a) and dotted lines in Fig. 2(b). (Bottom panel) The obtained spin-polarization, $P$, derived from the asymmetry between $I^+$ and $I^-$ using 0.21 as the value of effective Sherman function ($S_{eff}$) (see text). Error is indicated by bars. The quantization axis of the SARPES measurement is along x direction of the sample ($\bar{\Gamma}$–$\bar{K}$ direction in Fig. 2(a)). (Middle panel) Spin up ($I^{\uparrow}$: (red) solid line) and spin down ($I^{\downarrow}$: (blue) dashed line) spectra are obtained from the total spectrum ($I_{tot} = I^+ + I^-$, (black) thick line) and the polarization, $P$, by the usual procedure, $I^{\uparrow,\downarrow} = (1 \pm P)I_{tot}/2$. The angular resolution and energy resolution of the measurement are set as $\Delta\theta = \pm 0.70°$ and $\Delta E \sim 30$ meV ($E_p = 5$ eV, slit = 1.5, aperture = 2×3 and acceptance angle = ±7.0°) in this measurement.

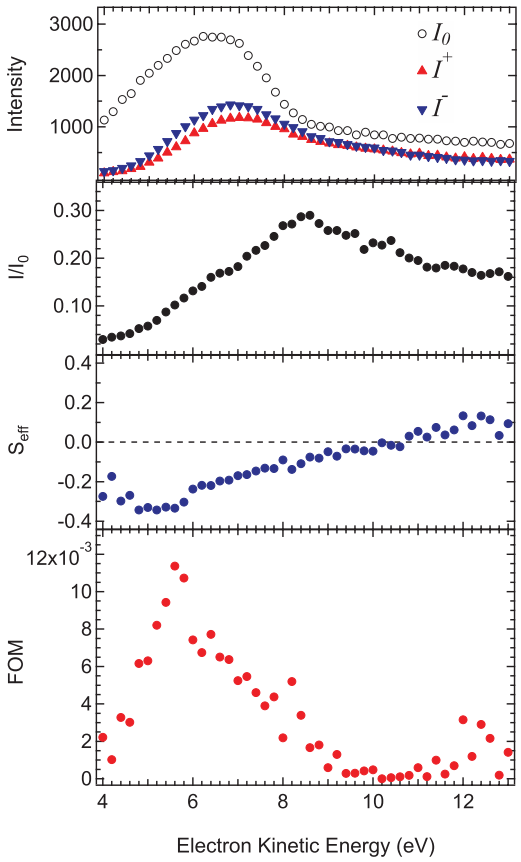


FIG. 4. (Color online) Intensity of reflected electrons by the positively ((red) up triangle: $I^+$) and negatively ((blue) down triangle: $I^-$) magnetized target as the function of electron kinetic energy (upper panel). The circle ($I_0$) is the total intensity of the impinged electrons onto the target position estimated by the measurement with the back channeltron ($CH_B$ in Fig. 1). From the observed electron intensities ($I^+$, $I^-$, and $I_0$) the electron reflectivity of the target $I/I_0 = (\frac{I^+ + I^-}{2})/I_0$ (second panel), and the asymmetry between positively and negatively magnetized target $A = (I^+ - I^-)/(I^+ + I^-)$ which is proportional to the effective Sherman function $S_{eff}$ (third panel) can be obtained. The total efficiency, the figure of merit (FOM) which is the products of the reflectivity and effective Sherman function is calculated as in the bottom panel (see text in detail).

The measurement has been done along $\bar{\Gamma}$–$\bar{M}$ of the sample (see Fig. 2) and the observed spin quantization axis is set along x direction ($\bar{\Gamma}$–$\bar{K}$ direction). The energy resolution and angular resolution are set at about 11 meV and ±0.35°, which corresponds to $E_p$= 2 eV, slit = 1.5, and aperture = 1×2 with the analyzer acceptance angle of ±7.0°. Figure 5(a) represents the observed SARPES spectra (spin up: (red) solid line and spin down: (blue) dashed line) as well as the total intensity ((black) thick solid line) spectra which are taken from −4° to 4° with 0.5° step using He discharge lamp ($h\nu = 21.22$ eV) at the sample temperature of 80 K. The acquisition time of each SARPES spectrum is 12 min. As in the figure the spin up and spin down states are clearly resolved and one can see the reverse of the spin up and spin down states intensities against the $\bar{\Gamma}$ point (0°) which is the characteristic of Rashba spin state.[21] This spin-polarization reversal with respect to the $\bar{\Gamma}$ point is much more directly seen in the angle-resolved spin-polarization spectra in Fig. 5(b). In the figure the mirror symmetric polarization change against $\bar{\Gamma}$ point (0°) is clearly seen. It is worth noting that almost completely zero polarization at the $\bar{\Gamma}$ point is good indication that our VLEED spin detector has very small instrumental asymmetry which does often matter in spin polarimeters. It is also to be noted that the polarization of the inner and outer surface states at ∼±1.5° and ∼±4°, are almost 100% in contrast to the smaller polarization less than 50% for the surface states observed in the previous SARPES measurement with the conventional Mott detector[21] resulting from the higher angular resolution of the present measurement.

From these SARPES spectra we can also make spin-resolved band dispersion maps as in Fig. 6. Figure 6(a) is the spin-integrated band dispersion map obtained from the total intensity spectra in Fig. 5(a). The characteristic band dispersion of the surface state of Bi(111) along $\bar{\Gamma}$–$\bar{M}$ direction is seen and in good agreement with the corresponding spin-integrated ARPES result that is indicated by a dashed box in Fig. 2(b). From Fig. 5(b) we made a spin-polarization map as in Fig. 6(b) and the clear polarization-reversal against $\bar{\Gamma}$ is directly seen. Because of the almost 100% polarization of the inner and outer surface states by the high-resolution SARPES measurement spin up and spin down states are

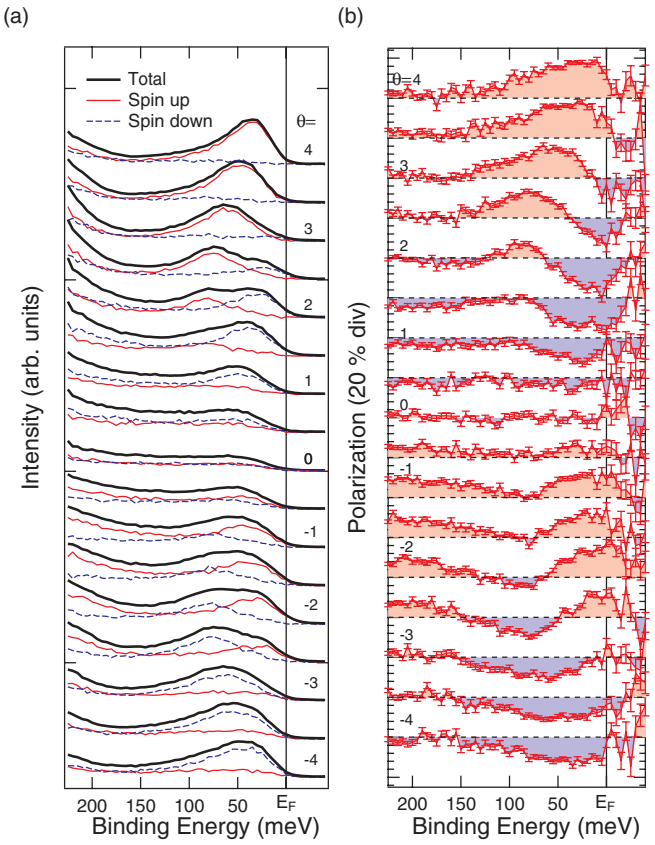


FIG. 5. (Color online) (a) SARPES spectra along $\bar{\Gamma}-\bar{\mathrm{M}}$ line of the surface states of Bi(111) film taken with He discharge lamp ($h\nu = 21.22$ eV). The SARPES spectra are from $-4^\circ$ to $4^\circ$ with the step of $0.5^\circ$. The observed area is indicated by the box in Fig. 2(b). Spin up and spin down states as well as the total intensity are indicated by (red) solid line, (blue) dashed line, and (black) thick solid line respectively. (b) Corresponding spin-polarization of (a). The spin-quantization axis is x direction ($\bar{\Gamma}$–$\bar{\mathrm{K}}$ direction in Fig. 2(a)). The maximum (minimum) spin polarization is almost $\pm 100\%$ at around $\pm 1.5^\circ$ and $\pm 4^\circ$.

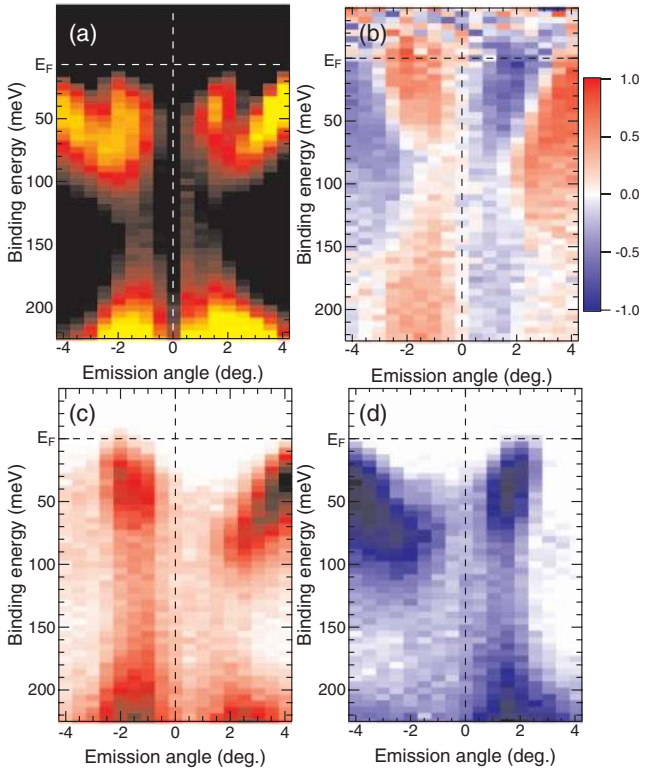


FIG. 6. (Color online) (a) Spin-integrated band mapping obtained from the total intensity of Fig. 5(a) which is in good agreement with the band dispersion obtained by the two-dimensional detector for the spin-integrated ARPES mode (box in Fig. 2(b)). (b) Spin-polarization mapping obtained from Fig. 5(b). The color scale indicates the spin-polarization. (c) and (d) The band mapping of (c) spin up and (d) spin down states that are obtained from the spin up and spin down SARPES spectra in Fig. 5(a).

explicitly resolved and now the dispersions of spin up and spin down bands can be separately obtained as in Figs. 6(c) and 6(d). The beautiful reflectional symmetry between Figs. 6(c) and 6(d) is due to the Rashba effect.

Although the energy resolution and angular resolution in the measurement of Figs. 5 and 6 are quite higher than in the ordinary SARPES measurement, we have further tried to check the best energy resolution of our ESPRESSO machine. For the purpose, we have measured the Fermi distribution curve from the Au polycrystal with the SARPES mode of ESPRESSO machine. The aperture and the slit size of this measurement has been set as $1\times 2$ (Angular30) and 0.2, respectively. The observed Fermi distribution curve at the sample temperature of about 10 K with using He discharge lamp is shown in Fig. 7 and quite high instrumental energy resolution of $\Delta E$ ~7.5 meV is achieved as in the figure. Though the acquisition time for the measurement was quite long (~12 h) and it is not practical for the usual measurement, if we use focused SR light from the undulator at the beamline it is expected that the count rate increases about 10 times higher than that of by the He discharge lamp and the high-energy resolution measurement will be available for the practical measurement.

As indicated in Table I, the best angular resolution for the SARPES measurement is about $\pm 0.09^\circ$ and one can select optimum angular resolution by changing the aperture size in accordance with the required wave vector resolution and the practical signal intensity which depends on the brilliance of the excitation light and photoionization cross section of the electronic states of sample. In practical use with our He discharge lamp (Gammadata Scienta VUV5000), the best angular resolution is $\pm 0.18^\circ$ which corresponds to about 0.013 $\text{Å}^{-1}$ and indicated by solid circle and vertical solid lines in Figs. 2(a) and 2(b), respectively. Note that the energy and angular resolution achieved by the ESPRSSO machine is the

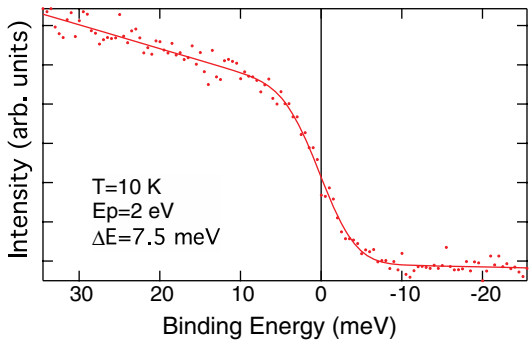


FIG. 7. (Color online) Fermi distribution curve measured by the ESPRESSO machine with Au polycrystal excited by the He discharge lamp ($h\nu = 21.22$ eV) at the sample temperature of about 10 K.

best for the SARPES measurement at present and also comparable to the ordinary high-resolution ARPES measurement and can be improved in principle with using much brilliant light sources such as the light from the undulator of third generation SR light sources or intense laser.

## IV. SUMMARY

We have developed a new spin- and angle-resolved photoelectron spectrometer named ESPRESSO machine with which one can obtain fine spin-structure of materials very efficiently. Favor of the high efficiency of the VLEED spin detector and high-energy resolution of the large hemispherical analyzer, very high-energy resolution and angular resolution ($\Delta E \sim 7.5$ meV and $\Delta\theta \sim \pm 0.18^{\circ}$) has been achieved in the SARPES measurement. The ESPRESSO machine, the combination of the highly efficient spin-integrated ARPES measurement by two-dimensional photoelectron detector and the efficient SARPES measurement by VLEED spin detector, is one of the best experimental tools to investigate the spin structure of magnetic materials, strongly spin-orbit coupled surfaces of non-magnetic materials, such as the Rashba spin-split systems and topological insulators which are the key materials of next generation electronic devices using the spin degree of freedom.

## ACKNOWLEDGMENTS

The authors acknowledge T. Maegawa and K. Okamoto for their help in the commissioning. Y. Takeichi is acknowledged for the collaboration during developing the ESPRESSO machine. This work was partly supported by KAKENHI (19340078), Grant-in-Aid for Scientific Research (B) of Japan Society for the Promotion of Science.

[1] P. D. Johnson, Rep. Prog. Phys. **60**, 1217 (1997).
[2] M. Hoesch, T. Greber, V. N. Petrov, M. Muntwiler, M. Hengsberger, W. Auwärter, and J. Osterwalder, J. Electron Spectrosc. Relat. Phenom. **124**, 263 (2002).
[3] T. Okuda, J. Lobo-Checa, W. Auwärter, M. Hoesch, V. N. Petrov, M. Hengsberger, A. Tamai, M. Morscher, A. Dolocan, C. Cirelli, M. Corso, M. Muntwiler, M. Roos, J. Osterwalder, and T. Greber, Phys. Rev. B **80**, 180404 (2009).
[4] S. Souma, A. Takayama, K. Sugawara, T. Sato, and T. Takahashi, Rev. Sci. Instrum. **81**, 096101 (2010).
[5] D. Hsieh, Y. Xia, L. Wary, D. Qian, A. Pal, J. H. Dil, J. Osterwalder, F. Meier, G. Bihlmayer, C. L. Kane, Y. S. Hor, R. J. Cava, and M. Z. Hasan, Science **323**, 919 (2009).
[6] S. Souma, K. Kosaka, T. Sato, M. Komatsu, A. Takayama, T. Takahashi, M. Kriener, K. Segawa, and Y. Ando, Phys. Rev. Lett. **106**, 216803 (2011).
[7] L. Moreschini, G. Ghiringhelli, K. Larsson, U. Veit, and N. Brookes, Rev. Sci. Instrum. **79**, 033905 (2008).
[8] C. Jozwiak, J. Graf, G. Lebedev, N. Andresen, A. K. Schmid, A. V. Fedorov, F. El Gabaly, W. Wan A. Lanzara, and Z. Hussain, Rev. Sci. Instrum. **81**, 053904 (2010).
[9] D. Tillmann, R. Thiel, and E. Kisker, Z. Phys. B **77**, 1 (1989).
[10] F. U. Hillebrecht, R. Jugblut, and E. Kisker, Phys. Rev. Lett. **65**, 2450 (1990).
[11] R. Bertacco, M. Merano, and F. Ciccacci, Appl. Phys. Lett. **72**, 2050 (1998).
[12] R. Bertacco, M. Marcon, G. Trezzi, L. Duò, and F. Ciccacci, Rev. Sci. Instrum. **73**, 3867 (2002).
[13] T. Okuda, Y. Takeichi, Y. Maeda, A. Harasawa, I. Matsuda, T. Kinoshita, and A. Kakizaki, Rev. Sci. Instrum. **79**, 123117 (2008).
[14] T. Okuda, Y. Takeichi, A. Harasawa, I. Matsuda, T. Kinoshita, and A. Kakizaki, Eur. Phys. J. Special Topics **169**, 181 (2009).
[15] A. Winkelmann, D. Hartung, H. Engelhard, C.-T. Chiang, and J. Kirschner, Rev. Sci. Instrum. **79**, 083303 (2008).
[16] F. U. Hillebrecth, F. M. Jungblut, L. Wiebusch, Ch. Roth, H. B. Rose, D. Knabben, C. Bethke, N. B. Weber, St. Manderia, U. Rosowski, and E. Kisker, Rev. Sci. Instrum. **73**, 1229 (2002).
[17] A. Nishide, A. A. Taskin, Y. Takeichi, T. Okuda, A. Kakizaki, T. Hirahara, K. Nakatsuji, F. Komori, Y. Ando, and I. Matsuda, Phys. Rev. B **81**, 041309 (2010).
[18] M. H. Berntsen, P. Palmgren, M. Leandersson, A. Hahlin, J. Åhlund, B. Wannberg, M. Måtensson, and O. Tjernberg, Rev. Sci. Instrum. **81**, 035104 (2010).
[19] S. He, S. Qiao, M. Arita, M. Nakatake, K. Shimada, H. Namatame, and M. Taniguchi, Activity Report of Hiroshima Synchrotron Radiation Center 2006, 2007, p. 79.
[20] T. Nagao, J. T. Sadowski, M. Saito, S. Yaginuma, Y. Fujikawa, T. Kogure, T. Ohno, Y. Hasegawa, S. Hasegawa, and T. Sakurai, Phys. Rev. Lett. **93**, 105501 (2004).
[21] T. Hirahara, K. Miyamoto, I. Matsuda, T. Kadono, A. Kimura, T. Nagao, G. Bihlmayer, E. V. Chulkov, S. Qiao, K. Shimada, H. Namatame, M. Taniguchi and S. Hasegawa, Phys. Rev. B **76**, 153305 (2007).
[22] K. Iori, K. Miyamoto, H. Narita, K. Sakamoto, A. Kimura, S. Qiao, K. Shimada, H. Namatame, and M. Taniguchi, Rev. Sci. Instrum. **77**, 013101 (2006).